A controlled variable inductor for an LCC-S compensated Wireless Power Transfer system

(Article begins on next page)

Magnetic Control of LCC-S Compensated Wireless Power Transfer System

Luigi Solimene
Politecnico di Torino
Dipartimento Energia
"G. Ferraris" (DENERG)
Torino, Italy
luigi.solimene@polito.it

Fabio Corti
Università di Perugia
Dipartimento di Ingegneria
Perugia, Italy
fabio.corti@unipg.it

Salvatore Musumeci
Politecnico di Torino
Dipartimento Energia
"G. Ferraris" (DENERG)
Torino, Italy
salvatore.musumeci@polito.it

Carlo Stefano Ragusa
Politecnico di Torino
Dipartimento Energia
"G. Ferraris" (DENERG)
Torino, Italy
carlo.ragusa@polito.it

Alberto Reatti
University of Florence
Dipartimento di Ingegneria
dell'Informazione (DINFO)
Firenze, Italy
alberto.reatti@unifi.it

Abstract— **This paper proposes the analysis of a magnetic controlled LCC-S compensated Wireless Power Transfer system that regulates the transferred load power by varying the magnetization level of a variable inductor. A steady-state analysis of the LCC-S compensation network is proposed, a design example of a controlled variable inductor for a 100 W Wireless Power Transfer system is described, and the simulation results are provided, considering the magnetic model of the variable inductor.**

Keywords— Wireless Power Transfer, Control, Variable Inductor.

I. Introduction

Wireless Power Transfer (WPT) is a suitable solution to avoid bulky cables during the charging process of electric devices [1]. This technology has been widely used in several applications, ranging from consumer electronics to electric vehicles [2]-[3]. For this latter application, wireless charging can potentially solve several problems related to cables. Several charging cables standards are available, such as Combo, CHAdeMO, Testa, GB/T[4]. Since the power charging rate is constantly increasing, reaching up to 400kW, one of the most critical elements of the charging infrastructure is the charging cables [5]. Higher cross-section and liquid cooling are required to maintain the temperature under safety levels, increasing costs and weights. EV wireless charging can be a suitable solution to these issues [6].

WPT systems can be divided into two main categories: Inductive Wireless Power Transfer (IWPT) and Capacitive Wireless Power Transfer (CWPT). Advantages and disadvantages have been extensively discussed in [7]. In this paper, the focus is placed on IWPT. The main limitation of WPT systems compared to wired solutions is the conversion efficiency. High leakage flux is presented since the power is transferred through an air gap, and high reactive power is required due to the coil's magnetic coupling. To this end, additional reactive components are used to create resonance and allow maximum power transfer. Several resonant compensations have been proposed over the years [8]. The most widely used topology is the Series-Series compensation. This topology is obtained by adding two capacitors in series with the coupled inductances. This topology operates as a current source and allows high conversion efficiency [9]. Higher-order compensations reduce the voltage/current stress and obtain different behaviour compared to the SS compensation for different load conditions. One of the most promising compensations is the LCC-S. Several works are focused on performance comparison with respect to the SS compensation [10]. Unlike the SS compensation, the LCC-S compensation acts as a voltage source. In [11], the output power and the conversion efficiency are compared under different load conditions. Since the SS compensation acts approximately as a current source, the output power increases linearly with the load resistance.

On the other hand, since the LCC-S compensation acts as a voltage source, the output power decreases with the load resistance. As shown in [11], another advantage of the LCC-S is the lower voltage stress across the components. An accurate power loss comparison between SS and LCC-S is presented in [12]. The results show the higher conversion efficiency of the LCC-S.

While the control of the SS compensation is relatively simple since it acts as a current source, the control of the LCC-S compensation is more complex. Most of the control strategies consist of varying a component to regulate the output voltage or current. For example, in [13], the two resonant capacitors are regulated using a MOSFET-type AC switch. Although this solution is simple, this approach requires many capacitors and switches, significantly increasing the costs of the system. In [14], an interesting approach that avoids the adoption of additional capacitors is proposed, using a switch-controlled capacitor. This approach enables the continuous variation of the equivalent capacitance within a specific range so that the compensation parameters can be fine-tuned according to the actual state of the system. However, an additional power MOSFET is required for each variable capacitor.

In this paper, a novel approach consisting of varying the resonant inductance is proposed. The main advantage of the proposed technique is the possibility to change only one component without adding several power components. This approach is usually defined as magnetic control, and it has been already widely used for the LCC [15][16][17]**Errore. L'origine riferimento non è stata trovata.**. The variable inductor is obtained through an auxiliary winding where a DC bias current generates a DC bias magnetic flux density inside the magnetic material, thus adjusting the material magnetic permeability by changing the DC operating point around the knee of the BH curve.

The paper is organized as follows. In Section II, the steady-state analysis of the LCC-S compensation is presented.

In Section III, the variable inductor design is presented. In Section IV, the simulation results using PLECS® software tool are shown. Finally, in Section V, the conclusions are derived.

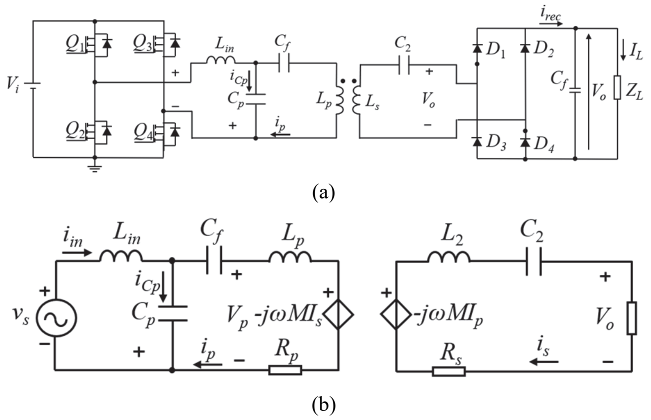

Fig. 1. Electric circuit. (a) DC-DC converter for IWPT with LCC-S compensation. (b) Equivalent electric circuit.

II. LCC-S COMPENSATION

In this Section, the analytical expression of the output power and conversion efficiency are derived and the case study is presented.

A. Analytical Analysis

The electric circuit of an LCC-S compensation is shown in Fig. 1. The relationship between capacitors and inductors, which allows obtaining the maximum power transfer and minimizing the reactive power circulating in the system, are

$$\omega_0 L_s = \frac{1}{\omega_0^2 C_s} \tag{1}$$

$$\omega_0 L_p = \frac{1}{\omega_0^2 C_p} \tag{2}$$

$$\omega_0 L_{in} = \omega_0 L_p - \frac{1}{\omega_0^2 C_f} \tag{3}$$

Let define

$$k_1 = L_{in} + L_p - \frac{1}{\omega^2 C_f} + \frac{C_p L_{in}}{C_f} - \omega^2 C_p L_{in} L_p \tag{4}$$

$$k_2 = \omega^2 M^2 + R_p R \tag{5}$$

$$R = R_L + R_s \tag{6}$$

Studying the circuit, the currents circulating in the circuit can be calculated as

$$I_s = \frac{MU_s}{k_1 R + j\omega\left(C_p L_{in} k_2 - M^2 - \dfrac{R_p R}{\omega^2} \right)} \tag{7}$$

$$I_p = \frac{RU_s}{k_2 k_5 + j\omega\left[R\left(L_{in} + L_p\right) - \dfrac{R}{\omega^2 C_f} - C_p L_{in}\left(\omega^2 L_p - \dfrac{R}{\omega C_f} \right) \right]} \tag{8}$$

$$I_{in} = \frac{\omega C_p U_s \left(\omega L_p R - jk_2 \right)}{k_2 k_5 + j\omega R\left[\left(\dfrac{1}{\omega^2 C_f} - L_{in} - L_p \right) - C_p L_{in}\left(\dfrac{1}{C_f} - \omega^2 L_p \right) \right]} \tag{9}$$

Thus, the output power $P_o = R_L\,|I_s|^2$ can be calculated as

$$P_o = \frac{\omega^2 M^2 U_s^2 R_L}{R^2 \omega^2 \left[L_{in} + L_p + \dfrac{L_{in} C_p}{C_f} k_3 - \dfrac{1}{\omega^2 C_f} \right]^2 + k_5^2 k_2^2} \tag{10}$$

The complex apparent power at the input of the resonant compensation is $S = U_s I_{in} = P_{in} + jQ_{in}$.

$$P_{in} = \Re\left\{ U_s I_{in} \right\} \tag{11}$$

Let define

$$k_3 = 1 - \omega^2 L_p C_f \tag{12}$$

$$k_4 = \omega^2 C_f \left(L_{in} + L^p \right) + \omega^2 L_{in} C_p k_3 - 1 \tag{13}$$

$$k_5 = 1 - \omega^2 L_{in} C_p \tag{14}$$

$$k_6 = 1 - \omega^2 L_p C_p \tag{15}$$

After many calculations, the input power can be calculated as

$$P_{in} = \frac{RU_s^2 \left[C_p k_2 k_4 + k_5 k_2 \left(C_p + k_6 C_f \right) \right]}{C_f \left(R^2 \omega^2 k_1^2 + k_2^2 k_5^2 \right)} \tag{16}$$

Thus, the transmission efficiency $\eta = P_o / P_{in}$ can be calculated as

$$\eta = \frac{\omega^2 M^2 R_L C_f}{R k_2 \left\{ C_p \left[\omega^2 C_f \left(L_{in} + L_p \right) \right] + \omega^2 L_{in} C_p k_3 - 1 \right\} + k_5 \left(C_p + C_f k_6 \right)} \tag{17}$$

If the system operates in resonance the equations (1), (2) and (3) are satisfied. Thus, the expression of the efficiency and output power can be simplified as follows

$$\eta = \frac{R_L \omega^2 M^2}{R\left(\omega^2 M^2 + RR_p \right)} \tag{18}$$

$$P_o = \frac{\omega^4 C_f^2 M^2 R_L U_s^2}{R^2 \left(\omega^2 C_f L_p - 1 \right)^2} \tag{19}$$

This latter equation can be rearranged to obtain a particular output power under resonant conditions. Thus, known the output power P_o and the resonant angular frequency ω_0, the capacitor C_f can be designed using

$$C_f = \frac{\omega L_p + \sqrt{\omega^2 \left(L_p^2 - M^2 R_L U_s^2 \right) - P_o R^2 L_p^2}}{\omega \left[R^2 L_p^2 - \omega^2 M^2 R_L U_s^2 \right]} \tag{20}$$

Under this condition, the input resistance $Z_{in} = R_{in} + j\,X_{in}$ is

$$R_{in} = \frac{(R_L + R_S)(\omega^2 C_f L_p - 1)^2}{\omega^2 C_f^2 (\omega^2 M^2 + RR_p)} \tag{21}$$

$$X_{in} = 0 \tag{22}$$

Thus, the maximum power transmission is achieved.

B. *Case Study*

In Table I, the constraints of the system analyzed in this paper are presented.

TABLE I
CIRCUIT PARAMETER

Parameter	Value	Description
f	85 kHz	Operating Frequency
V_I	24 V	DC Input Voltage
P_o	50 W	Output power
k	0.2	Coupling coefficient
L_p, L_s	50 µH	Primary and Secondary Inductance
R_p, R_s	0.2 Ω	Primary and Secondary Parasitics
R_L	10 Ω	Load Resistance

Using (1)-(3), the resonant components can be designed. The values are summarized in Table II.

TABLE I
SCIRCUIT PARAMETER

Parameter	Value
C_f	82 nF
L_{in}	7.4 µH
C_p	471 nF
C_s	70 nF

The proposed control strategy consists of regulating the output power varying the inductance L_{in}. Using (16) and (17), the output power and the conversion efficiency in steady-state condition can be evaluated.

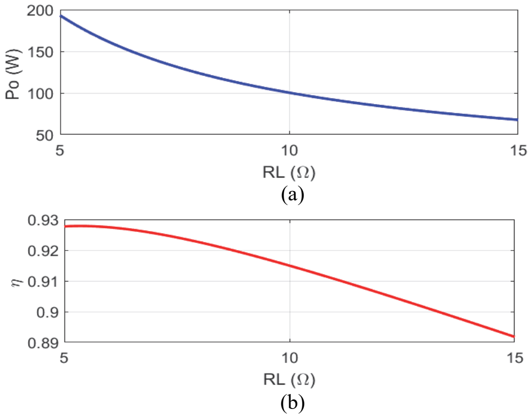

Fig. 2. Resonant compensation behaviour for different load resistance. (a) Output power. (b) Transmission efficiency.

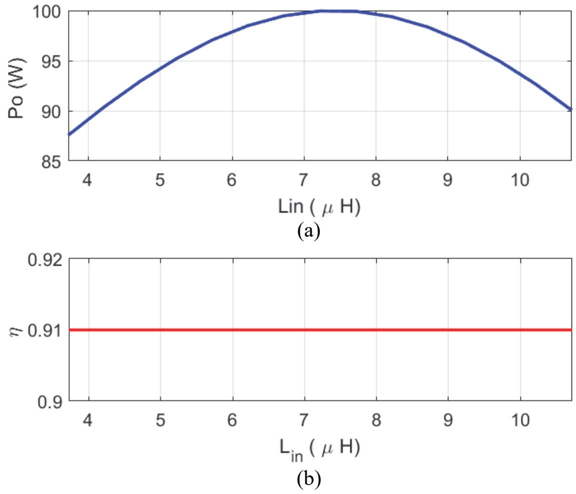

Fig. 3. Resonant compensation behaviour under variable inductance L_{in}. (a) Output power. (b) Transmission efficiency.

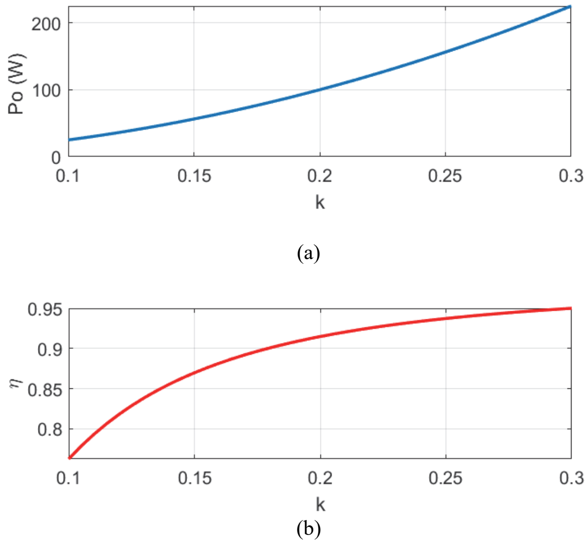

Fig. 4. Resonant compensation behaviour for different coupling coefficients. (a) Output power. (b) Transmission efficiency.

III. Variable Inductor Design Procedure

In this Section, the procedure adopted for designing a controlled variable inductor is described. The variation of the inductance value can be achieved operating on the incremental permeability of the magnetic core material, which is defined as

$$\mu_\Delta = \frac{\partial B}{\partial H}. \tag{23}$$

Different magnetic field strength values lead the magnetic material to operate in three different regions of the magnetization curve, from a linear region, where the differential permeability shows a near-constant profile, to a roll-off region, in which the permeability rapidly decreases, finally to a saturation region, where the minimum value of the differential permeability is obtained, and the material is fully saturated. Fig. 4 represents the magnetization curve and the incremental inductance profile of a Mn-Zn ferrite, highlighting the different operating regions.

In this paper, the topology adopted to realize the controlled variable inductor is composed of a double E core with the main winding placed on the central leg and connected to other components of the LCC-S compensation network and two auxiliary winding placed on the outer legs of the core [19]. By controlling the direct current value in the auxiliary windings, the applied magnetomotive force in the core is varied, and thus the magnetic field strength in the magnetic material is controlled. The auxiliary windings are connected in series with opposite polarity to force the DC magnetic flux path only in the outer legs of the double E core. Instead, the central leg operates in the linear region of the magnetization curve and is designed to assure the component exhibits a linear behaviour when excited with the AC magnetomotive force swing.

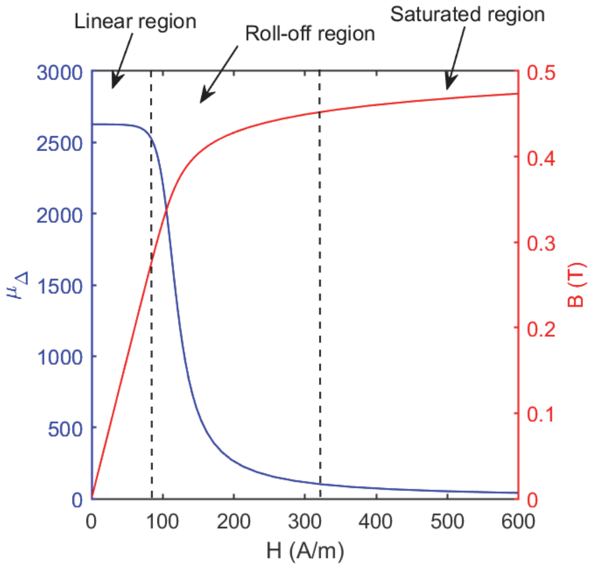

Fig. 5. Magnetization curve of a a Mn-Zn ferrite. The red line represents the B-H curve and the blue line represents the related incremental inductance profile. The three different operating regions of soft magnetic material are highlighted.

To this end, a concentrated air gap is adopted in the central leg of the selected core. Fig. 5(a) represents the arrangement of the considered core geometry. The equivalent reluctance model represented in Fig. 5(b) is adopted to compute the incremental inductance profile referred to the main winding [20].

The air gap reluctance and the ferromagnetic path reluctance can be described as constant terms by

$$\Re_{\mathrm{fe,c}} = \frac{l_{\mathrm{fe,c}}}{\mu_{\mathrm{fe,in}} S_{\mathrm{fe,c}}}, \tag{24}$$

$$\Re_{\mathrm{g}} = \frac{l_{\mathrm{g}}}{\mu_0 S_{\mathrm{g}}}, \tag{25}$$

while the reluctance of the outer leg's ferromagnetic path can be described as a function of the magnetomotive force applied by the auxiliary windings:

$$\Re_{\mathrm{fe,l}}(N_{\mathrm{DC}} I_{\mathrm{DC}}) = \frac{l_{\mathrm{fe,l}}}{\mu_{\mathrm{fe}}(N_{\mathrm{DC}} I_{\mathrm{DC}}) S_{\mathrm{fe,l}}}. \tag{26}$$

The equivalent reluctance referred to main winding is defined as

$$\Re_{\mathrm{eq}}(N_{\mathrm{DC}} I_{\mathrm{DC}}) = \Re_{\mathrm{fe,c}} + \Re_{\mathrm{g}} + 0.5 \cdot \Re_{\mathrm{fe,l}}(N_{\mathrm{DC}} I_{\mathrm{DC}}), \tag{27}$$

and thus, the incremental inductance can be computed as

$$L(N_{\mathrm{DC}} I_{\mathrm{DC}}) = \frac{N_{AC}^2}{\Re_{\mathrm{eq}}(N_{\mathrm{DC}} I_{\mathrm{DC}})} \tag{28}$$

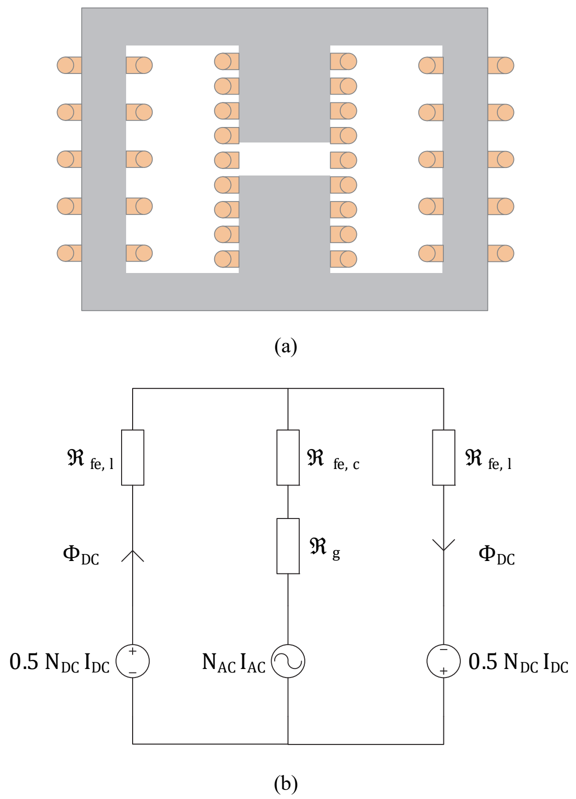

Fig. 6. Description of the core and winding configuration for the variable inductor design. (a) Detail of the double E core gapped configuration. (b) Equivalent reluctance circuit.

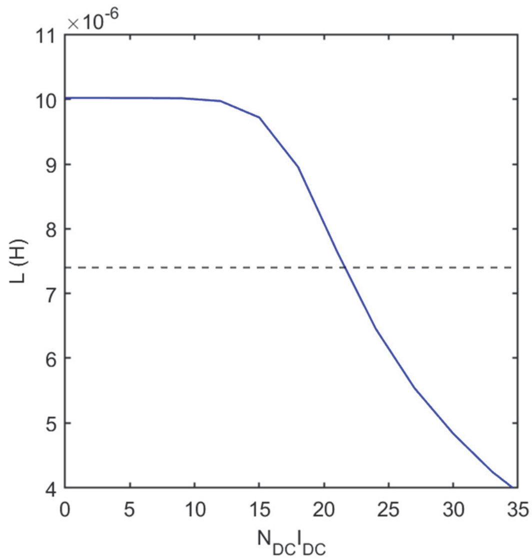

Fig. 7. Incremental inductance profile of the proposed variable inductor, as a function of the magnetomotive force if the auxiliary windings.

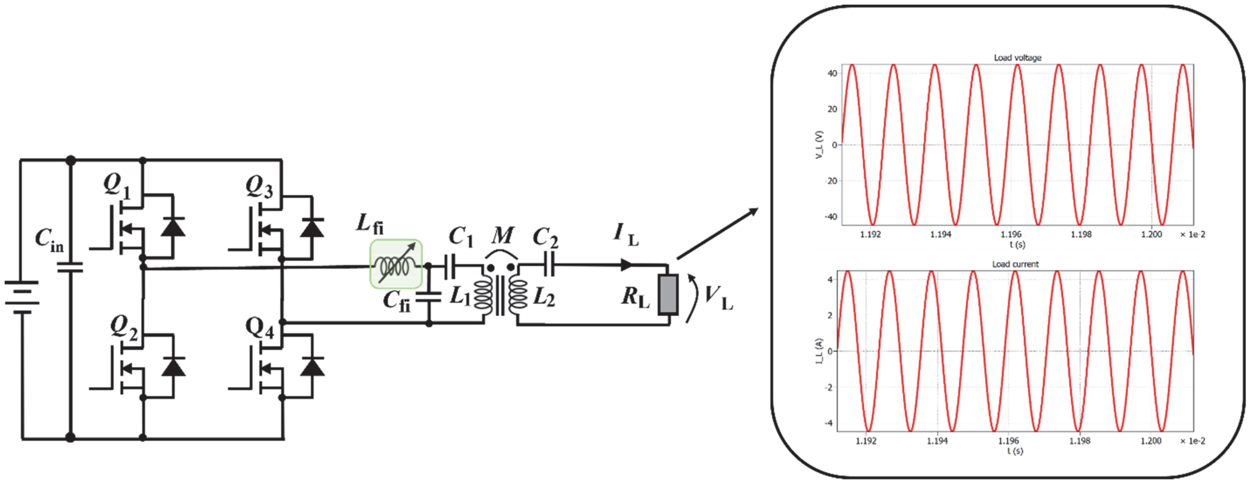

(a) (b)

Fig. 8. (a) Electrical circuit or the setup adopted in the Plecs simulation. (b) Detail of the load voltage and current waveform during 100 W operation.

To obtain a variable inductance profile suitable for the specification of the designed LCC-S compensation topology, a N87 double E 32/6/9 core is selected, with a 0.25 mm gap on the central leg, 5 turns on the main winding and 5 turns of the auxiliary windings, equally split on the outer legs.
The supply of the auxiliary windings is realized with a synchronous buck converter, and the current value to control the incremental inductance value is obtained through a PI regulator. Fig. 6 represents the incremental inductance profile of the designed variable inductor as a function of the magnetomotive force of the auxiliary windings.

IV. Simulation Results

The presented LCC-S compensated WPT system has been tested with dedicated software tool (PLECS®), assuming the first harmonic approximation on the load side, as represented in Figure 8. The simulated output load voltage and current waveforms are represented in the same Figure, when an average load power of 100W is transferred. At the previously specified switching frequency, input voltage, and load level, by varying the magnetization current in the auxiliary windings of the variable inductor, the average load power can be regulated, as represented in Figure 9. The magnetizing current level suddenly reaches the target value, and a 0.5A current ripple is observed due to the magnetic unbalance of the outer legs of the core when operating in saturation, which causes a non-zero electromotive force on the series of the two windings, and due to the small impedance of the magnetization circuit. However, this does not represent an issue for the average load power transmission, as shown in the upper graph of Figure 9. Moreover, Figure 10 represents the operating region on the magnetization curve of the outer leg's core material in the saturated and the unsaturated region. Due to the polarity of the applied DC magnetic flux and the addition of the air gap, the central leg instead operates in the linear region of the magnetization curve.

V. Conclusions

In conclusion, the presented paper proposes the analysis of a LCC-S compensated WPT system, focusing on the magnetic control of the output power.

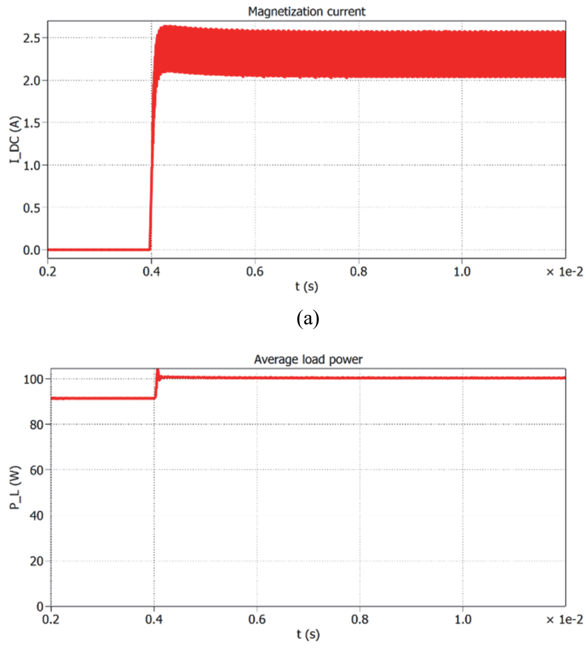

(a)

(b)

Fig. 9. (a) Simulated magnetization current waveform. (b) Related average power transferred to the load

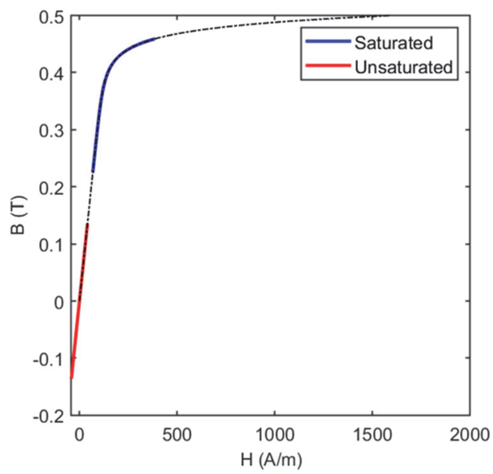

Fig. 10. Operating regions of the outer leg's magnetic material in saturated and unsaturated conditions.

The target is obtained by adopting a controlled variable inductor, adequately designed to operate in a range of inductance values controlled by regulating the current of an auxiliary magnetizing winding. The theoretical analysis of the LCC-S compensation is supported by the simulation results of a 100 W WPT system, considering the magnetic model of a N87 ferrite double E-core variable inductor.

REFERENCES

[1] C. C. Mi, G. Buja, S. Y. Choi and C. T. Rim, "Modern Advances in Wireless Power Transfer Systems for Roadway Powered Electric Vehicles," in *IEEE Transactions on Industrial Electronics*, vol. 63, no. 10, pp. 6533-6545, Oct. 2016, doi: 10.1109/TIE.2016.2574993.

[2] Locorotondo E, Corti F, Pugi L, Berzi L, Reatti A, Lutzemberger G. Design of a Wireless Charging System for Online Battery Spectroscopy. *Energies*. 2021; 14(1):218. https://doi.org/10.3390/en14010218

[3] S. R. Khutwad and S. Gaur, "Wireless charging system for electric vehicle," *2016 International Conference on Signal Processing, Communication, Power and Embedded System (SCOPES)*, 3-5 Oct. 2016, Paralakhemundi, India, pp. 441-445, doi: 10.1109/SCOPES.2016.7955869.

[4] B. Al-Hanahi, I. Ahmad, D. Habibi and M. A. S. Masoum, "Charging Infrastructure for Commercial Electric Vehicles: Challenges and Future Works," in *IEEE Access*, vol. 9, pp. 121476-121492, 2021, doi: 10.1109/ACCESS.2021.3108817.

[5] H. Tu, H. Feng, S. Srdic and S. Lukic, "Extreme Fast Charging of Electric Vehicles: A Technology Overview," in *IEEE Transactions on Transportation Electrification*, vol. 5, no. 4, pp. 861-878, Dec. 2019, doi: 10.1109/TTE.2019.2958709.

[6] M. R. Khalid, I. A. Khan, S. Hameed, M. S. J. Asghar and J. -S. Ro, "A Comprehensive Review on Structural Topologies, Power Levels, Energy Storage Systems, and Standards for Electric Vehicle Charging Stations and Their Impacts on Grid," in *IEEE Access*, vol. 9, pp. 128069-128094, 2021, doi: 10.1109/ACCESS.2021.3112189.

[7] Corti F, Reatti A, Wu Y-H, Czarkowski D, Musumeci S. Zero Voltage Switching Condition in Class-E Inverter for Capacitive Wireless Power Transfer Applications. *Energies*. 2021; 14(4):911. https://doi.org/10.3390/en14040911

[8] A. Mahesh, B. Chokkalingam and L. Mihet-Popa, "Inductive Wireless Power Transfer Charging for Electric Vehicles–A Review," in *IEEE Access*, vol. 9, pp. 137667-137713, 2021, doi: 10.1109/ACCESS.2021.3116678.

[9] Corti F, Reatti A, Nepote A, Pugi L, Pierini M, Paolucci L, Grasso F, Grasso E, Nienhause M. A Secondary-Side Controlled Electric Vehicle Wireless Charger. *Energies*. 2020; 13(24):6527. https://doi.org/10.3390/en13246527

[10] Y. Chen, H. Zhang, C. -S. Shin, K. -H. Seo, S. -J. Park and D. -H. Kim, "A Comparative Study of S-S and LCC-S Compensation Topology of Inductive Power Transfer Systems for EV Chargers," *2019 IEEE 10th International Symposium on Power Electronics for Distributed Generation Systems (PEDG)*, 2019, pp. 99-104, doi: 10.1109/PEDG.2019.8807684.

[11] F. Corti *et al*., "A Comprehensive Comparison of Resonant Topologies for Magnetic Wireless Power Transfer," *2020 IEEE 20th Mediterranean Electrotechnical Conference (MELECON)*, 2020, pp. 582-587, doi: 10.1109/MELECON48756.2020.9140657.

[12] Z. She, S. Chen, Y. Chen, Y. Zhang, H. Li and Y. Tang, "Efficiency Analysis of LCC-S and S-S Inductive Power Transfer Considering Switching Device and Component Losses," *2020 IEEE 9th International Power Electronics and Motion Control Conference (IPEMC2020-ECCE Asia)*, 2020, pp. 2956-2960, doi: 10.1109/IPEMC-ECCEAsia48364.2020.9368208.

[13] Y. Chen, H. Zhang, S. -J. Park and D. -H. Kim, "A Switching Hybrid LCC-S Compensation Topology for Constant Current/Voltage EV Wireless Charging," in *IEEE Access*, vol. 7, pp. 133924-133935, 2019, doi: 10.1109/ACCESS.2019.2941652.

[14] K. Li, W. Ding and J. Yuan, "An LCC-S Compensated Wireless Power Transfer System with Dual Switch-Controlled Capacitors for Multi-Frequency Receivers," *2021 IEEE Energy Conversion Congress and Exposition (ECCE)*, 2021, pp. 5828-5833, doi: 10.1109/ECCE47101.2021.9595811.

[15] Y. Wei, D. Woldegiorgis and A. Mantooth, "Variable Resonant and Magnetizing Inductor Control for LLC Resonant Converter," *2020 IEEE 11th International Symposium on Power Electronics for Distributed Generation Systems (PEDG)*, 2020, pp. 149-153, doi: 10.1109/PEDG48541.2020.9244466.

[16] Y. Wei, Q. Luo and A. Mantooth, "Comprehensive analysis and design of LLC resonant converter with magnetic control," in *CPSS Transactions on Power Electronics and Applications*, vol. 4, no. 4, pp. 265-275, Dec. 2019, doi: 10.24295/CPSSTPEA.2019.00025.

[17] V. S. Costa, M. S. Perdigão, A. S. Mendes and J. M. Alonso, "Evaluation of a variable-inductor-controlled LLC resonant converter for battery charging applications," *IECON 2016 - 42nd Annual Conference of the IEEE Industrial Electronics Society*, 2016, pp. 5633-5638, doi: 10.1109/IECON.2016.7793916.

[18] W. Ma, X. Xie and S. Jiang, "LLC resonant converter with variable resonant inductor for wide LED dimming range," *2017 IEEE Applied Power Electronics Conference and Exposition (APEC)*, 2017, pp. 2950-2957, doi: 10.1109/APEC.2017.7931116.

[19] J. M. Alonso, M. Perdigão, M. A. Dalla Costa, S. Zhang, e Y. Wang, "Variable inductor modeling revisited: The analytical approach", *2017 IEEE Energy Conversion Congress and Exposition (ECCE)*, 2017, pp. 895–902. doi: 10.1109/ECCE.2017.8095880

[20] S. Musumeci, L. Solimene, and C. S. Ragusa. "Identification of DC Thermal Steady-State Differential Inductance of Ferrite Power Inductors" *Energies* 2021, vol. 14, no. 13: 3854. https://doi.org/10.3390/en14133854.